

# Planetary Systems in a Star Cluster II: intermediate-mass black holes and planetary systems

Francesco Flammini Dotti<sup>1,2</sup>, M.B.N. Kouwenhoven<sup>1\*</sup>, Qi Shu<sup>3,4</sup>, Wei Hao<sup>5</sup>  
and Rainer Spurzem<sup>6,7,3†</sup>

<sup>1</sup>*Department of Physics, School of Science, Xi'an Jiaotong-Liverpool University, 111 Ren'ai Rd., Suzhou Dushu Lake Science and Education Innovation District, Suzhou Industrial Park, Suzhou 215123, P.R. China*

<sup>2</sup>*Department of Mathematical Sciences, University of Liverpool, Liverpool L69 3BX, UK*

<sup>3</sup>*Kavli Institute for Astronomy and Astrophysics at Peking University, 5 Yiheyuan Rd., Haidian District, 100871, Beijing, China*

<sup>4</sup>*Department of Astronomy, School of Physics, Peking University, Yiheyuan Lu 5, Haidian Qu, 100871, Beijing, China*

<sup>5</sup>*Max Planck Institut für Astrophysik, Karl-Schwarzschild-Str. 1 85741 Garching, Germany*

<sup>6</sup>*National Astronomical Observatories and Key Laboratory of Computational Astrophysics, Chinese Academy of Sciences, 20A Datun Rd., Chaoyang District, 100012, Beijing, China*

<sup>7</sup>*Astronomisches Rechen-Institut, Zentrum für Astronomie, University of Heidelberg, Mönchhofstrasse 12–14, 69120, Heidelberg, Germany*

Last updated 24 July 2020

## ABSTRACT

Most stars form in dense stellar environments. It is speculated that some dense star clusters may host intermediate-mass black holes (IMBHs), which may have formed from runaway collisions between high-mass stars, or from the mergers of less massive black holes. Here, we numerically explore the evolution of populations of planets in star clusters with an IMBH. We study the dynamical evolution of single-planet systems and free-floating planets, over a period of 100 Myr, in star clusters without an IMBH, and in clusters with a central IMBH of mass  $100 M_{\odot}$  or  $200 M_{\odot}$ . In the central region ( $r \lesssim 0.2$  pc), the IMBH's tidal influence on planetary systems is typically 10 times stronger than the average neighbour star. For a star cluster with a  $200 M_{\odot}$  IMBH, the region in which the IMBH's influence is stronger within the virial radius ( $\sim 1$  pc). The IMBH quenches mass segregation, and the stars in the core tend to move towards intermediate regions. The ejection rate of both stars and planets is higher when an IMBH is present. The rate at which planets are expelled from their host star rate is higher for clusters with higher IMBH masses, for  $t < 0.5t_{\text{rh}}$ , while remains mostly constant while the star cluster fills its Roche lobe, similar to a star cluster without an IMBH. The disruption rate of planetary systems is higher in initially denser clusters, and for wider planetary orbits, but this rate is substantially enhanced by the presence of a central IMBH.

**Key words:** stars: solar-type – stars: planetary systems – planets: dynamical evolution and stability – stars: statistics – stars: black holes

## 1 INTRODUCTION

Planetary systems are believed to be common in star clusters (e.g., Mayo et al. 2018; Thompson et al. 2018). In order to understand the origin and dynamical evolution of planetary systems and rogue planets in star clusters, it is necessary to carefully study the effect of their environments, i.e., that of the star-forming region in which they were born (e.g., Lada & Lada 2003) and in which they remain the first million

years, and that of the Galactic tidal field, the open cluster, or the globular cluster in which they may spend the billions of years that follow.

In this study we analyse the effect of a central IMBH on the evolution of planetary systems and on populations of free-floating planets in star clusters. The differential gravitational force of a central IMBH affects the evolution of both binary star systems and planetary systems. A massive IMBH, located in or near the centre of the star cluster affects not only the densest regions of the star cluster, but when sufficiently massive, it can dominate the evolution of planetary systems throughout the entire star cluster. In order to understand the evolution of planetary systems in star clusters,

\* Contact e-mail: [t.kouwenhoven@xjtlu.edu.cn](mailto:t.kouwenhoven@xjtlu.edu.cn)

† Research Fellow at Frankfurt Institute for Advanced Studies (FIAS)

it is thus interesting and necessary to quantify the effect of a central IMBH on a planetary system, and to compare this to the contribution of neighbouring stars.

Many of the currently known black holes have been identified through their gravitational influence on neighbouring objects or through accretion of gas. Unlike stellar-mass black holes (e.g., A0620-00/V616, [Cantrell et al. 2010](#)) and supermassive black holes (e.g., SgrA\*, [Schödel et al. 2002](#)), IMBHs have not yet been directly observed. Several candidate IMBHs have been identified in star clusters. These include HLX-1 in ESO 243-49 ([Farrell et al. 2009](#)), and the candidate IMBHs in NGC 4395 ([den Brok et al. 2015](#), although its mass is between that of a SMBH and an IMBH), 47 Tuc ([Koliopanos 2017](#)), and NGC 6624 ([Perera et al. 2017](#)). [Koliopanos \(2017\)](#) estimate that globular clusters can host IMBH up to  $\sim 1000 M_{\odot}$ . A promising IMBH candidate was recently identified by [Lin et al. \(2020\)](#). The IMBH candidate was identified through a stellar tidal disruption event, and is estimated to have a mass of  $50\,000 M_{\odot}$ . Gravitational waves signatures of IMBH candidates in star clusters may substantially increase the number of known IMBH candidates in star clusters in the near future (e.g., [Abbott et al. 2017](#)).

The existence of IMBHs in star clusters is predicted by several theoretical models. Among these, the model involving a stellar runaway collision is the least controversial. When the local stellar density in the centre of a star cluster is sufficiently high, runaway stellar collisions can ultimately result in the formation of an IMBH within roughly five relaxation times (e.g., [Portegies Zwart & McMillan 2002](#); [Portegies Zwart et al. 2004](#); [Gürkan et al. 2004](#); [Freitag et al. 2006](#)). The IMBHs formed through this channel typically have masses of  $\sim 10^2 M_{\odot}$ . Mergers of stellar-mass black holes can also result in IMBHs, with masses of up to  $\sim 10^5 M_{\odot}$ . [Miller & Hamilton \(2002\)](#) show that more massive black holes ( $> 50 M_{\odot}$ ) sink towards a star cluster's centre and merge to form an IMBH, while less massive black holes may escape within  $\sim 10^7$  Myr (e.g., [Sigurdsson & Hernquist 1993](#); [Kulkarni et al. 1993](#); [de Vita et al. 2018](#)). Population III stars are thought to have had substantially higher masses than Population I and II stars. It is possible to obtain black holes with masses over  $200 M_{\odot}$  (e.g., [Madau & Rees 2001](#); [Ricotti & Ostriker 2004](#); [Wheeler & Johnson 2011](#)) and likely have a central IMBH ([Reinoso et al. 2018](#)). This IMBH forms faster ( $\lesssim 3$  Myr) than any other scenario. Finally, the most massive IMBHs may have formed from primordial stars of masses  $\sim 10^5 M_{\odot}$ , in dark matter mini-haloes, at redshift  $z > 15$  (e.g., [Haiman et al. 1996](#); [Yoshida et al. 2003](#)).

In a previous study ([Flammini Dotti et al. 2020, 2019](#)) we explored how the star cluster environment changes the architecture of a complex planetary system (i.e., a multi-planetary system with a range in planetary masses). Strong encounters with neighbouring stars can result in instabilities in a planetary system, which may result in orbital re-configurations or planetary ejections (e.g., [Spurzem et al. 2009](#); [Boley et al. 2012](#)). Even mild perturbations and tidal perturbations can affect short-period planets in the system, resulting in ejection and/or scattering between different planets (e.g., [Hao et al. 2013](#); [Flammini Dotti et al. 2019](#)). The effect of a stellar encounter on a planetary system depends on the relative speed of the encountering star, the local stellar density, the effective encounter strength, and

the orbital architecture and mass spectrum of the planets in the planetary system.

Upon ejection from their host planetary system, free-floating planets (FFPs) typically obtain a velocity-at-infinity in the range  $0.1 - 10 \text{ km s}^{-1}$ . The velocity-at-infinity tends to be somewhat higher for prompt ejection (as a direct result of star-planet encounters) than for delayed ejection (as a result of a planet-planet scattering); see [Malmberg et al. \(2011\)](#). Once escaped, a FFP may be captured by another star, especially in case of prompt ejection ([Kouwenhoven et al. 2010](#); [Malmberg et al. 2011](#); [Moeckel & Clarke 2011](#); [Parker & Quanz 2012](#); [Perets & Kouwenhoven 2012](#)) or remain in the star cluster, within an estimated time scale of many millions of years (e.g., [Hurley & Shara 2002](#); [Parker & Quanz 2012](#); [Craig & Krumholz 2013](#)).

[Veras & Raymond \(2012\)](#) show that the FFP population in the Galactic field is not the result of decaying planetary systems alone, but that close encounters in star clusters are most likely the primary cause of FFPs. Observations of FFPs are limited, but extrapolations suggested that FFPs are common in the Galactic disk. Estimates range from two Jupiter-mass FFPs per every main-sequence star ([Sumi et al. 2011](#)), to  $10^5$  FFPs with masses between  $10^{-8} M_{\odot}$  and  $10^{-2} M_{\odot}$  per star ([Strigari et al. 2012](#)). A large contribution of FFP observations comes from the micro-lensing detections of FFP ([Mao & Paczynski 1991](#); [Gould & Loeb 1992](#); [Abe et al. 2004](#); [Beaulieu et al. 2006](#); [Gaudi 2012](#)). Only several FFPs have been unambiguously detected thus far (e.g., CFBDSIR 2149-0403 and PSO J318-22; see [Delorme et al. 2012](#); [Liu et al. 2013](#)). A recent, and more comprehensive analysis by [Mróz et al. \(2017\)](#) finds that [Sumi et al. \(2011\)](#) greatly overestimates the abundance of free-floating Jupiter-mass planets in the Galactic field, and also point out that the findings of [Sumi et al. \(2011\)](#) do not match predictions from planet formation theories ([Veras & Raymond 2012](#); [Ma et al. 2016](#)) and that they are inconsistent with surveys of young clusters ([Scholz et al. 2012](#); [Peña Ramírez et al. 2012](#); [Mužić et al. 2015](#)). Using a much larger sample of microlensing events, [Mróz et al. \(2017\)](#) reveal a significantly lower abundance, of roughly one free-floating Jupiter-mass planet or wide-orbit Jupiter-mass planet for every four main-sequence star in the Galactic field.

Earlier works on IMBHs in star clusters focus on the relation between the stellar dynamics and a central IMBH. Here, we aim to relate the presence of an IMBH to the evolution of planetary systems and free-floating debris. We focus on the lower-mass end of the IMBH mass distribution. We also investigate how the presence of an IMBH affects the stellar dynamics, and how this contributes to the (in)stability of planetary systems. This paper is organised as follows. In §2 we introduce our numerical method and the initial conditions. In §3 we describe our results: we first obtain analytical estimates for the tidal influence of an IMBH planetary systems; we subsequently analyse disruption rates and escape rates, and how these depend on the properties of the star cluster, the planetary systems, and the central IMBH. Finally, we summarise and discuss our findings in §4.

## 2 METHODOLOGY AND INITIAL CONDITIONS

### 2.1 Initial conditions - star cluster and IMBH

We study open clusters with  $N = 10\,000$  stellar members. We draw stellar positions and velocities from the [Plummer \(1911\)](#) model, with an initial virial radius of  $r_{\text{vir}} = 1$  pc. The modeled star clusters have a typical stellar density of  $10^4$  stars per cubic parsec, which is higher than that of most known open clusters in the Milky Way, comparable to that of newborn open clusters, and lower than that of globular clusters. Star clusters with different initial stellar densities are discussed in Section 3.3.2. The clusters are initialized with a virial ratio  $Q = 1/2$ , where  $Q = |T/U|$ ,  $T$  is the cluster's total kinetic energy and  $U$  the total gravitational energy. Stellar masses are drawn from the ([Kroupa 2001](#)) initial mass distribution in the mass range  $M_* = 0.08 - 100 M_\odot$ . We adopt the standard solar neighbour tidal field, corresponding to the Solar orbit in the Milky Way. We do not include primordial binaries, and we ignore the presence of any gas remaining from the star-formation process. The initial conditions for the reference models are listed in Table 1.

The stellar population is initialised with an age of 30 Myr. We use this approach as a more realistic initial condition for IMBH formation ([Koliopanos 2017](#)). During the first  $\sim 30$  Myr, massive stars ( $\gtrsim 25 M_\odot$ ; [Fryer 1999](#)) evolve into a black hole, favouring the IMBH formation scenario discussed above. Consequently, the  $N$ -body simulations are initialized with a 30-Myr old stellar population with an evolved mass function. The most massive object at the start of each simulation, excluding the IMBH, is typically a stellar-mass black hole with a mass between  $50 M_\odot$  and  $70 M_\odot$ . Following others studies of IMBH's in star clusters, we adopt a stellar metallicity of  $Z = 0.001$  (e.g., [Hurley 2007](#); [Arca-Sedda 2016](#)). All models are evolved for  $t = 100$  Myr, which corresponds to roughly four half-mass relaxation times. In order to enhance statistical significance, we carry out an ensemble of ten realisations for each star cluster model.

We carry out simulations with and without a central IMBH, to investigate the effect of the presence of an IMBH on both the stellar and planetary population (see Table 1).

The models contain IMBHs with masses of  $M_{\text{BH}} = 0 M_\odot$  (i.e., no IMBH),  $M_{\text{BH}} = 100 M_\odot$  and  $M_{\text{BH}} = 200 M_\odot$ . The latter two correspond to the lower-mass end of IMBH mass spectrum, and represent IMBHs formed through stellar runaway collisions and/or subsequent merging between black holes. IMBHs are initialised at rest at the centre of the star cluster. This is expected because massive objects (the IMBH, or its progenitors) tend to sink towards the core and oscillate around the centre of the star cluster (e.g., [Miller & Hamilton 2002](#); [Wrobel et al. 2016](#); [Arca-Sedda 2016](#)). Note that in our study we do not make attempts to model or explain the formation history the central IMBH. Forming a central IMBH through a runaway collision process requires the cluster to evolve for at least a relaxation time (e.g., [Portegies Zwart & McMillan 2002](#); [Portegies Zwart et al. 2004](#); [Gürkan et al. 2004](#); [Freitag et al. 2006](#)), and during this time, the stellar mass function evolves not only due to the process of stellar evolution, but also due to escape events, and the merger events that are responsible for the origin of the IMBH itself.

### 2.2 Initial conditions - planets

We study the dynamical evolution of two populations of planets: (i) planets in orbit around a star s), and (ii) free-floating planets. Their main properties are summarised in Table 1. The abbreviations used in this paper are listed in Table 2.

In each star cluster, five hundred randomly selected stars are assigned a Jupiter-mass planetary companion. Semi-major axes are drawn from a uniform logarithmic distribution in the interval  $1 \text{ AU} < a < 100 \text{ AU}$ . In Section 3.3.3 we describe two additional models, where we consider the intervals  $a = 1 - 10 \text{ AU}$  and  $a = 10 - 100 \text{ AU}$ . All planets are initialised on circular ( $e = 0$ ) orbits. Hereafter, we refer to such a star-planet systems as a BP when it is gravitationally bound to the star cluster, and as an eBP when it has escaped from the star cluster.

In addition, we add five hundred Jupiter-mass free-floating planets (FFPs) to each star cluster. Their initial positions and velocities are drawn from distributions that are statistically identical to those of the stars, and are therefore initially in virial equilibrium with the stellar population.

Stellar encounters may disrupt planetary systems and thus generate free-floating planets. In order to obtain insight into the evolution of a population of initially-virialized free-floating planets and planets expelled from their host planetary system, we distinguish these two populations. We refer to (primordial) free-floating planets in the star cluster as FFPs, and to the population of planets in the cluster that was expelled from their host systems as BFPs. When these free-floating planets have escaped from the star cluster, we refer to them as eFFPs, eBFPs, respectively.

Stars without a planetary companion, including those that have lost their companion at an earlier time, are referred to as NHSs when they are gravitationally bound to the star cluster, and as eNHS when they have escaped. We do not describe planetary capture events, which are rare, and refer to Shu et al. (submitted) for a detailed discussion.

### 2.3 Numerical method

We use NBODY6++GPU ([Wang et al. 2015b](#); [Wang et al. 2016](#)) to model the dynamical evolution of star clusters by direct  $N$ -body simulation. NBODY6++GPU is based on the earlier  $N$ -body codes NBODY6 ([Aarseth 1999](#)) and NBODY6++ ([Spurzem 1999](#)), but the main difference is its ability to use graphical processing units (GPUs). The parallelisation is achieved via MPI (Message Passing Interface; [Tapamo 2009](#)) and OpenMP on the top level, and parallel use of many GPU cores on the bottom level. The code uses the Ahmad-Cohen neighbour scheme ([Ahmad & Cohen 1973](#)): regular forces from distant particles are parallelized using the GPU, while irregular forces from neighbour particles are computed in parallel on multi-cores on the CPU using OpenMP. The GPU implementation in NBODY6++GPU provides a significant acceleration, especially for the long-range (regular) gravitational forces. The simulation data are stored in HDF5 format (see, e.g., [Portell de Mora et al. 2011](#)), which is a highly efficient storage scheme that can be used for reconstructing the dynamical properties of the star clusters with high temporal and spatial accuracy for further analysis ([Cai et al. 2015](#)). Stellar evolution in NBODY6++GPU is modelled using the pre-

**Table 1.** Initial conditions for the star clusters: the model identification (column 1, using the syntax C-Q0-IMBH mass), the initial total star cluster mass (column 2), the IMBH mass (column 3), the initial crossing time and relaxation time (columns 4 and 5), the initial core radius (column 6), the initial half-mass radius (column 7), and other relevant parameters (column 8).

Model ID	$M_{\text{cl}}$ $M_{\odot}$	$M_{\text{IMBH}}$ $M_{\odot}$	$t_{\text{cr}}$ Myr	$t_{\text{rh}}$ Myr	$r_{\text{c}}$ pc	$r_{\text{hm}}$ pc	Other parameters
C50M000	$5.95 \times 10^3$	0	0.18	27.15	0.39	0.78	BP=500, FFP=500
C50M100	$6.05 \times 10^3$	100	0.18	27.44	0.24	0.79	$a = 1 - 100$ AU, $e = 0$
C50M200	$6.15 \times 10^3$	200	0.18	27.74	0.15	0.80	Ensemble size = 10

**Table 2.** Abbreviations used in this study, for populations of particles that are gravitationally bound to the star cluster (column 2) and for populations of particles that have escaped from the star cluster (column 3).

Particle	Cluster member	Escaped from cluster
Intermediate-mass black hole	IMBH	—
Star-planet system	BP	eBP
Primordial free-floating planet	FFP	eFFP
Bound free-floating planet; a free-floating planet that was in orbit around a star at $t = 0$	BFP	eBFP
Non-host stars (including stars that lost their planet)	NHS	eNHS

descriptions of Hurley et al. (2000, 2002, 2005), for single stellar evolution (Hurley et al. 2013a), for binary stellar evolution (Hurley et al. 2013b), and for fallback and kicks for the formation of stellar remnants is modelled using the prescriptions of (respectively for fallbacks and kicks, Hobbs et al. 2005; Belczynski et al. 2002). In recent years, LIGO data helped in the updates of NBODY6++GPU and NBODY7 codes (see, e.g., Belczynski et al. 2008; Banerjee 2020, and references therein).

Following Spurzem et al. (2009), we model planetary systems containing only a single planet. The dynamical evolution of such star-planet binary systems can be accurately modelled using the algorithms in NBODY6++GPU, with the main difference of an upgraded code version, improved to use planetary particles and a central IMBH simultaneously and efficiently. As the star cluster evolves, stars can escape from the cluster through tidal evaporation or dynamical ejection. Following Aarseth (2010), we identify particles with a cluster-centric radius of  $r > 2r_{\text{tidal}}$  as escapers, where  $r_{\text{tidal}} \propto M_{\text{cl}}^{1/3}(t)$  is the instantaneous tidal radius of the star cluster, which is evaluated in NBODY6++GPU following the prescriptions of Aarseth (2010).

### 3 RESULTS

#### 3.1 Theoretical estimates

In this section we estimate the impact of a central IMBH presence on planetary systems in a star cluster. We quantify the relative contributions of the tidal force exerted by the IMBH and by the nearest neighbour star at different locations in the star cluster. We obtain analytical estimates for two models: for the homogeneous spherical model and the Plummer (1911) model. For comparison with the simulations, we also present a brief analysis on the stability of a planetary system in the presence of an isolated IMBH.

##### 3.1.1 Formalism

Let  $\mu$  be the mass of the planet,  $m_{\star}$  the mass of the host star, and  $m_n$  be the mass of a neighbouring body. Let  $r_{\star}$  be the distance between the star and the planet, and  $r_n$  be the

distance between the star and the neighbouring body. The gravitational force between the star and the planet is then

$$F_{\star} = \frac{G\mu m_{\star}}{r_{\star}^2}, \quad (1)$$

and the tidal force that is exerted by the neighbouring body on the planet is then, to first order approximation:

$$F_n = \frac{2G\mu m_n r_{\star}}{r_n^3}. \quad (2)$$

The ratio between the tidal force exerted by the neighbouring body on the planet and the force exerted by the host star on the planet is

$$f = \frac{F_n}{F_{\star}} = 2 \left( \frac{m_n}{m_{\star}} \right) \left( \frac{r_{\star}}{r_n} \right)^3. \quad (3)$$

In a star cluster that contains an IMBH, planetary systems are affected by both the neighbouring stars and by the IMBH. Let  $M_B$  and  $M_n$  be the masses of the IMBH and the nearest neighbour star, respectively. Let  $R_B$  and  $R_n$  be the distances to the IMBH and to the nearest neighbour star, respectively. The ratio between the two tidal forces is then

$$g = \frac{f_B}{f_N} = 2 \frac{M_B}{M_n} \left( \frac{R_n}{R_B} \right)^3. \quad (4)$$

When  $g = 1$ , the tidal forces exerted by the IMBH on the planet is equal to that of the neighbour star. When  $g < 1$  ( $g > 1$ ), the neighbour star's tidal force is stronger (weaker) than that of the IMBH. When inserting  $g = 1$  we obtain

$$\frac{M_n}{M_B} = 2 \left( \frac{R_n}{R_B} \right)^3. \quad (5)$$

Star clusters are evolving systems, in which a planetary system experiences rapid changes in the tidal forces it experiences. The expressions above, however, can provide rough estimates about whether the tidal force experienced by a planetary system is dominated by the IMBH or by the neighbour stars.

If the assumption is made that the nearest neighbour star to the planetary system exerts a tidal force that is much larger than that of the more distant nearest neighbours, the expressions above can be used to make estimates for a star



cluster environment. In this case,  $M_n = \langle m \rangle$  can be interpreted as the average mass of the nearest neighbour, and  $R_n$  as the average distance to the nearest neighbour. Let  $d$  be the distance from the planetary system to the star cluster centre. For star clusters in which the black hole is in the centre of the star cluster ( $d = R_B$ ), Eq. (5) can be used to obtain the distance from the star cluster centre at which the tidal contribution of the IMBH is equal to that of the nearest neighbour star, under the assumption that both  $R_n$  and  $M_n$  are independent of  $d$ :

$$d = R_B = R_n \left( \frac{2M_B}{M_n} \right)^{1/3}. \quad (6)$$

In the more general case of a star cluster, the properties of the nearest neighbour stars may depend on location. In these cases, solving Eq. (4), with  $R_B = d$ ,  $R_n = R_n(d)$  (a radial density profile), and  $M_n = M_n(d)$  (mass segregation) may result in zero, one, or multiple solutions when solving  $g(d) = 1$ .

### 3.1.2 The homogenous spherical star cluster

Consider a spherical and homogeneous star cluster of radius  $R_{\text{cl}}$  containing  $N$  stars and an IMBH of mass  $M_B$  at its centre. Let  $d$  again be the distance of a planetary system to the centre of the star cluster.

The typical distance between the planetary system and its nearest neighbour is  $R_n \approx N^{-1/3} R_{\text{cl}}$  when the planetary system is inside the star cluster, and  $R_n \approx d - R_{\text{cl}}$  when the planetary system is outside the star cluster ( $d > R_{\text{cl}}$ ). The tidal ratio, as defined in Eq. (4) is then

$$g(d) \approx \begin{cases} 2 \frac{M_B}{M_{\text{cl}}} \left( \frac{R_{\text{cl}}}{d} \right)^3 & d \leq R_{\text{cl}} \\ 2 \frac{M_B}{\langle m \rangle} \left( 1 - \frac{R_{\text{cl}}}{d} \right)^3 & d > R_{\text{cl}} \end{cases} \quad (7)$$

When considering a planetary system inside the star cluster ( $d < R_{\text{cl}}$ ), Eq. (6) becomes

$$d = R_B = R_{\text{cl}} \left( \frac{2M_B}{N \langle m \rangle} \right)^{1/3} = R_{\text{cl}} \left( \frac{2M_B}{M_{\text{cl}}} \right)^{1/3}, \quad (8)$$

where  $M_{\text{cl}}$  is the total mass of the star cluster.

This allows us to estimate the region in which the tidal force of the IMBH dominates over that of the a planetary system's neighbour stars. For a homogeneous cluster containing  $N = 10\,000$  stars and  $R_{\text{cl}} = 1$  pc, we obtain

$$R_{\text{bh}} = 0.069 \left( \frac{M_B}{M_{\odot}} \right)^{1/3} \text{ pc}. \quad (9)$$

Here we have adopted the average stellar mass  $\langle m \rangle \approx 0.6 M_{\odot}$  of the Kroupa (2001) IMF.

For a star cluster with a central IMBH of mass of  $M_{\text{BH}} = 100 M_{\odot}$ , the radius of the sphere in which the IMBH dominates the tidal evolution of the planets is  $R_{\text{bh}} = 0.320$  pc. This means that roughly 32% of the stars in the star cluster fall in this category. For star clusters with an IMBH mass of  $M_B = 200 M_{\odot}$  the value increases to  $R_{\text{bh}} = 0.403$  pc, representing roughly 40% of the stars in the cluster.

### 3.1.3 The Plummer model

The Plummer (1911) model provides a more accurate description of star clusters than that described in Section 3.1.2. The mass density profile for the Plummer model is

$$\rho_m(d) = \frac{3M_{\text{cl}}}{4\pi\alpha^3} \left( 1 + \frac{d^2}{\alpha^2} \right)^{-5/2} \quad (10)$$

(see, e.g., Heggie & Hut 2003), where  $\alpha = 3\pi r_{\text{vir}}/16$  is the scale radius, and  $M_{\text{cl}}$  the total mass of the star cluster (excluding the IMBH). The number density of stars can be obtained by dividing Eq. (10) by the average stellar mass:  $\rho_*(d) = \rho_m(d)/\langle m \rangle$ .

At a distance  $d$  from the cluster centre, the average distance between a planetary system and its nearest neighbour star is then

$$R_n(d) = \rho_*(d)^{-1/3} = \left( \frac{4\pi\alpha^3}{3N} \right)^{1/3} \left( 1 + \frac{d^2}{\alpha^2} \right)^{5/6}, \quad (11)$$

where we have used  $M_{\text{cl}} = \langle m \rangle N$ . Substituting the above expressions into Eq. (4), and assuming that the IMBH is located at the centre of the star cluster, we obtain

$$g(d) = \frac{8\pi}{3} \frac{M_{\text{BH}}}{M_{\text{cl}}} \left( \frac{\alpha}{d} \right)^3 \left( 1 + \frac{d^2}{\alpha^2} \right)^{5/2}. \quad (12)$$

Near the cluster centre (i.e., near the IMBH), where  $d \ll \alpha$ , the above expression reduces to

$$g(d) = \frac{8\pi}{3} \frac{M_{\text{BH}}}{M} \left( \frac{\alpha}{d} \right)^3 \gg 1. \quad (13)$$

In the region surrounding the IMBH, the influence of the IMBH is much stronger than that of the nearest neighbour star. Far away from the star cluster ( $d \gg \alpha$ ), Eq. (12) reduces to

$$g(d) = \frac{8\pi}{3} \frac{M_{\text{BH}}}{M} \left( \frac{d}{\alpha} \right)^2 \gg 1, \quad (14)$$

which tells us that the tidal force of the IMBH on the planetary system is much larger than that of the nearest neighbour.

The minimum of  $g(d)$  occurs at  $d_{\text{min}} = (3/2)^{1/2} \alpha \approx 1.22\alpha$ . Note that the location of this minimum is independent of the number of stars in the cluster, the mass of the black hole, and the average stellar mass. At this minimum, the IMBH has the smallest relative contribution to the tidal force (with respect to that of the nearest neighbours) experienced by a planetary system. At this location the tidal ratio is

$$g(d_{\text{min}}) \approx 29.2 \frac{M_{\text{BH}}}{M_{\text{cl}}}. \quad (15)$$

The tidal ratio  $g(d_{\text{min}})$  is smaller than unity when the IMBH mass is less than 3.4% of the total stellar mass of the star cluster. Note that, when the  $M_{\text{BH}} > 0.034 M_{\text{cl}}$ , then  $g(d) > 1$  throughout the entire cluster. In other words, the tidal force exerted by an IMBH tends to dominate the evolution of planetary systems at all locations in the star cluster.

The contributions of neighbouring stars and the IMBH to the tidal force on a planetary system when  $g(d) = 1$ . Eq. (12) has no solution of  $g(d) = 1$  when  $M_{\text{BH}} > 0.034 M_{\text{cl}}$ , has one solution when  $M_{\text{BH}} = 0.034 M_{\text{cl}}$ , and has two solutions when  $M_{\text{BH}} < 0.034 M_{\text{cl}}$ . The latter case is most realistic for both open clusters and globular clusters.

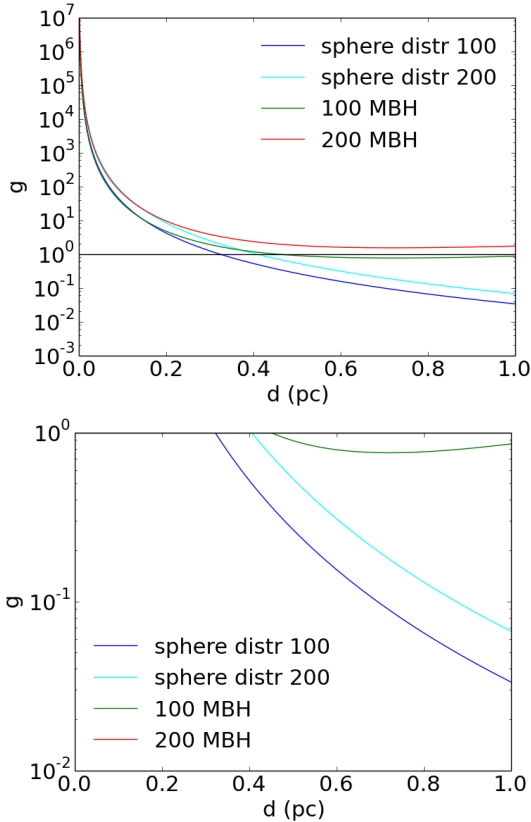


**Figure 1.** The tidal influence ratio,  $g(d)$ , for the spherical homogeneous star cluster (light-blue and dark-blue curves) and for the Plummer models (green and blue curves), for  $M_{\text{BH}} = 100 M_{\odot}$  and  $M_{\text{BH}} = 200 M_{\odot}$  (*top panel*). The black horizontal line at  $g(d) = 1$  indicates the transition between tidal domination by the IMBH and tidal domination by neighbour stars. The region with  $g < 1$  is shown separately in the bottom panel.

### 3.1.4 Applications

The derivations above allow us to make compare the tidal influence of IMBHs in star clusters numerically. In these examples we consider (i) homogeneous spheres with  $R_{\text{cl}} = 1$  pc, and (ii) Plummer models with  $r_{\text{vir}} = 1$  pc (i.e.,  $\alpha = 0.589$  pc). Both clusters have a total stellar mass of  $M_{\text{cl}} = 5950 M_{\odot}$  (excluding the IMBH). In both models, we calculate the tidal ratio  $g(d)$  for star clusters with a central IMBH masses of  $M_{\text{BH}} = 100 M_{\odot}$  and  $M_{\text{BH}} = 200 M_{\odot}$ .

The top panel Figure 1 shows a comparison between the ratios  $g(d)$  for the four different models. In all models  $g(d) \gg 1$  in the central regions of the cluster. In the cores of the star cluster ( $d \lesssim 0.1$  pc), the tidal force exerted by the IMBH is orders or magnitude larger than that of the neighbour stars. For the spherical homogeneous star clusters, IMBHs tend not to dominate the tidal force experienced by planetary systems in the outer regions of the star cluster. For the Plummer models, the IMBH plays an important role throughout the entire star cluster. Note that for  $M_{\text{BH}} \gtrsim 200 M_{\odot}$ ,  $g(d) > 1$  throughout the entire star cluster.

Even though in some regions of the star cluster the tidal force exerted by a central IMBH on a planetary system is larger, and sometimes even many orders of magnitude larger, than that of the typical neighbour star, the

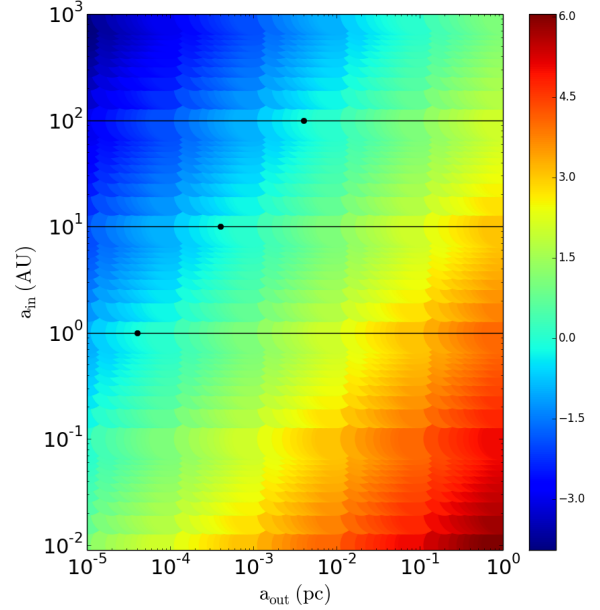


**Figure 2.** Stability map of planetary systems, with a semi-major axis ( $a_{\text{in}}$ ) at a distance from an IMBH ( $a_{\text{out}}$ ). The three horizontal lines represent the reference values for the semi-major axes used in our study, and the black dots are where the instability starts for each of them. The colours indicate the values of  $\log(p_{\text{out}}/p_{\text{crit}})$ . The blue regions are most unstable, while the red regions are most stable.

IMBH itself may not be the direct cause of the disruption of planetary systems. It can, however, induce orbital changes that may result in the decay of multi-planet systems, or that may facilitate disruption by neighbour stars. We discuss the stability criteria of a planetary system orbiting an isolated IMBH. In this case, the configuration can be treated as a hierarchical triple system. We define the star-planet system as the inner binary, while the planetary system orbiting the IMBH as the outer binary. The quantities  $a_{\text{in}}$ ,  $a_{\text{out}}$  represent the semi-major axes of the inner and outer orbits,  $e_{\text{in}}$  and  $e_{\text{out}}$  the inner and outer eccentricities, and  $q_{\text{in}} = m_{\text{p}}/m_{\text{star}}$  and  $q_{\text{out}} = M_{\text{BH}}/(m_{\text{star}} + m_{\text{p}})$  the inner and outer mass ratios. The periastron separation of the outer orbit is  $p_{\text{out}} = a_{\text{out}}(1 - e_{\text{out}})$ . For simplicity, we only consider co-planar orbits, i.e., systems with inclinations  $i_{\text{in}} = 0^\circ$  and  $i_{\text{out}} = 0^\circ$ . [Mardling & Aarseth \(2001\)](#) numerically obtained stability criteria for hierarchical three-body systems, and find the empirical formula

$$p_{\text{crit}} = 2.8 a_{\text{in}} \frac{1 - e_{\text{out}}}{1 + e_{\text{in}}} \left[ (1 + q_{\text{out}}) \frac{1 + e_{\text{out}}}{(1 - e_{\text{out}})^{\frac{1}{2}}} \right]^{0.4}, \quad (16)$$

where systems with  $p_{\text{out}} > p_{\text{crit}}$  are considered stable.

Figure 2 shows a map of the ratio  $p_{\text{out}}/p_{\text{crit}}$  as a function of  $a_{\text{out}}$  and  $a_{\text{in}}$ , for the circular, co-planar case with  $M_{\text{BH}} = 100 M_{\odot}$  IMBH, a Solar-mass star and a Jupiter-mass planet. The blue regions in Figure 2 indicate configurations that are unstable (i.e., those that result in disruption of the planetary system). Note that these are configurations that are unlikely to occur in realistic systems. The substantial

increase in disruptions of planetary systems in the presence of an IMBH is therefore an indirect, rather than a direct consequence of the IMBH.

The impact of an encounter on a planetary system (in terms of its ability to cause permanent changes) is determined by (i) the kinematic properties of the encountering star, and (ii) the properties of the planetary system. An encounter with a stellar neighbour can be characterised through its impulsiveness, adiabaticity, and the hyperbolic eccentricity (e.g., [Flammini Dotti et al. 2019](#), and references therein). A planetary system experiences many of such encounters, depending on the local stellar density. While there is only one IMBH in the star cluster, its interaction with the planetary system is permanent. The interaction with the IMBH can thus be considered as an encounter that lasts for billions of years. The impact of this interaction can be substantial, especially when  $g(d) > 1$ .

We remind the reader that the derivations above has several approximations, uses averaged values for stellar masses and stellar separations. It is also important to note that the presented values represent the initial conditions, and do not take into account the dynamical evolution of the star cluster. However, these results provide useful insight into the importance of IMBHs on the dynamical evolution of planetary systems star clusters.

### 3.2 Star cluster evolution

Although the focus of this study is the effect of an IMBH on the evolution of planetary systems in star clusters, it is important to first consider how an IMBH considers the star cluster itself, as the latter can have a considerable indirect effect on how planetary systems evolve these environments.

#### 3.2.1 Evolutionary timescales

To understand how the environment of planetary systems in star clusters is shaped by interactions between the stellar population and the IMBH it is useful to consider the relevant timescales at which these changes occur. Stars cross the star cluster at a timescale that is comparable to the crossing time,

$$t_{\text{cr}} = \sqrt{\frac{2r_{\text{hm}}^3}{GM_{\text{cl}}}} \quad (17)$$

(e.g., [Spitzer 1987](#); [Lamers et al. 2005](#); [Binney & Tremaine 2008](#)). Here  $r_{\text{hm}}$  is the half-mass radius,  $G$  is the gravitational constant, and  $M_{\text{cl}}$  the total mass of the star cluster. The relaxation time is defined by the time over which, for most stars in the cluster, the effect of stellar encounters on the velocity of stars becomes comparable to the star's initial velocity:

$$t_{\text{rh}} = \frac{0.138N_s}{\ln \Lambda} \sqrt{\frac{r_{\text{hm}}^3}{GM_{\text{cl}}}} \quad (18)$$

(e.g., [Spitzer 1987](#); [Khalisi et al. 2007](#)), where  $\Lambda$  depends on the stellar density distribution of the cluster (as in [Spitzer 1987](#)): the corresponding value is  $\Lambda = 0.11N_s$  ([Giersz & Spurzem 1994](#)).

The energy equipartition timescale (often referred to as the mass segregation timescale) describes how long it takes

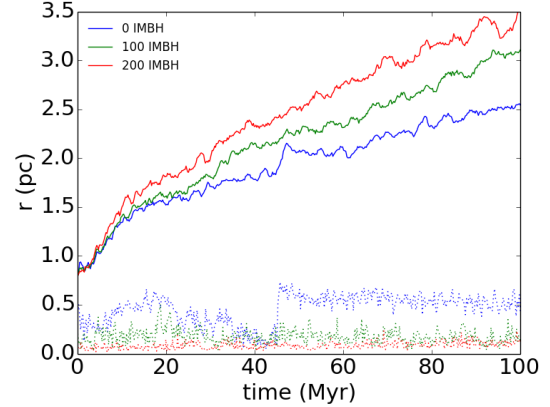


**Figure 3.** The evolution half-mass radii (*solid curves*) and core radii (*dotted curves*), for models C50M00 (*blue*), model C50M100 (*green*), and model C50M200 (*red*); see also Table 1.

for different stellar populations within the star cluster to exchange energy (see, e.g., [Spurzem & Takahashi 1995](#); [Mouri & Taniguchi 2002](#)):

$$t_{\text{ms}} = \frac{m_s}{\langle m \rangle} t_{\text{rh}} \quad (19)$$

([Khalisi et al. 2007](#)), where  $m_s$  is the stellar mass under consideration and  $\langle m \rangle$  is the average stellar mass. The mass segregation mechanism appears to be quenched in globular clusters that contain a central IMBH ([Gill et al. 2008](#)).

The core collapse timescale depends on both the star cluster's initial density profile and on the properties of the binary population (e.g., [Hurley et al. 2007](#)). [Heggie & Hut \(2003\)](#) define the core collapse timescale as

$$t_{\text{cc}} \approx \frac{v^3}{\nu G^2 \langle m \rangle^2 n \log \Lambda}, \quad (20)$$

where  $\nu$  is a parameter related to the relaxation timescale and varies in time,  $v$  is the typical stellar speed in the core,  $\langle m \rangle$  the typical stellar mass in the core and  $n$  the density number in the core. For the Plummer model,  $t_{\text{cc}} \approx 15 t_{\text{rh,core}}$ , (see, e.g., [Portegies Zwart et al. 2010](#)).

#### 3.2.2 Global properties

The presence of a central IMBH affects the global properties of a star cluster that can be observed in multiple ways: (i) the evolution of the core radius, (ii) the speed at which the energy equipartition process operates, and (iii) the delay, or prevention, of core collapse. Moreover, the kinematics of all constituent populations of the star cluster is directly and/or indirectly affected by the presence of the IMBH.

In observational astronomy, the core radius of a star cluster is often defined as the radius at which the surface brightness drops to one-half its central value (e.g., [Wilkinson et al. 2003](#)). Different definitions are used for theoretical and computational studies, where the core radius is normally derived from the three-dimensional mass density profile of the star cluster ([Casertano & Hut 1985](#)). [Aarseth \(2001\)](#) introduced the density radius as a measurement of the size of a star cluster in the NBODY6 code. The stellar density at the location of each star is estimated from the mass of the sphere containing the six nearest neighbour stars, while the

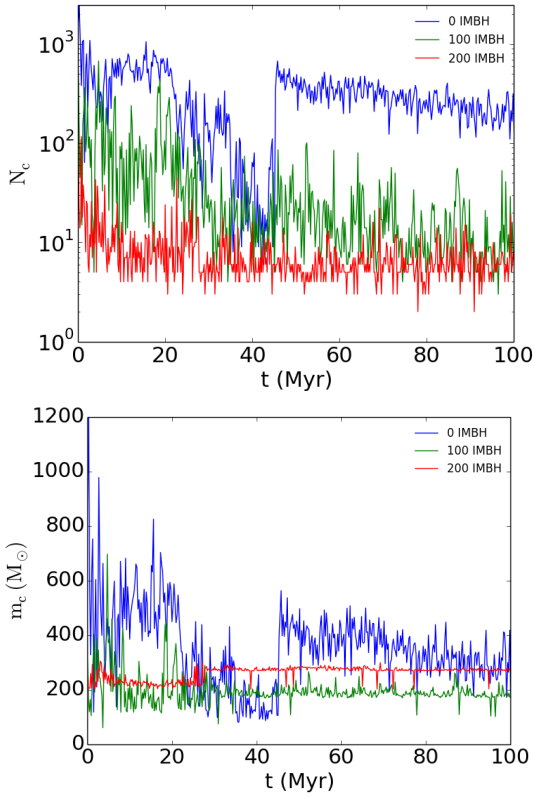


**Figure 4.** Evolution of the number of stars in the cluster core (*top*) and the enclosed mass in the cluster core (*bottom*), for the three reference models.

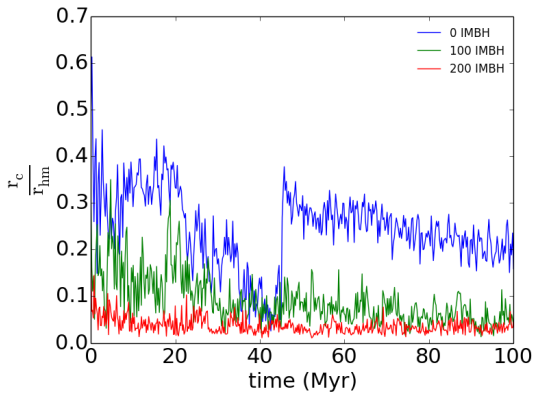


**Figure 5.** Evolution of the ratio between the core radius and half-mass radius for the three reference models (c.f. Figure 3).

density centre is defined as the density-weighted mean position of the stars, following the prescription of [Casertano & Hut \(1985\)](#).

The impact of IMBHs on the evolution of our modelled star clusters is shown in Figure 3. The IMBH makes a considerable contribution to the mass profile, and consequently the Lagrangian radii, in the core region. The interaction of the IMBH with surrounding stars causes an accelerated expansion of the star cluster. During the first few million years, the half-mass radius grows faster for the models containing an IMBH. The core particles escape in a shorter time due to the IMBH’s gravitational kicks, and tends to enlarge the

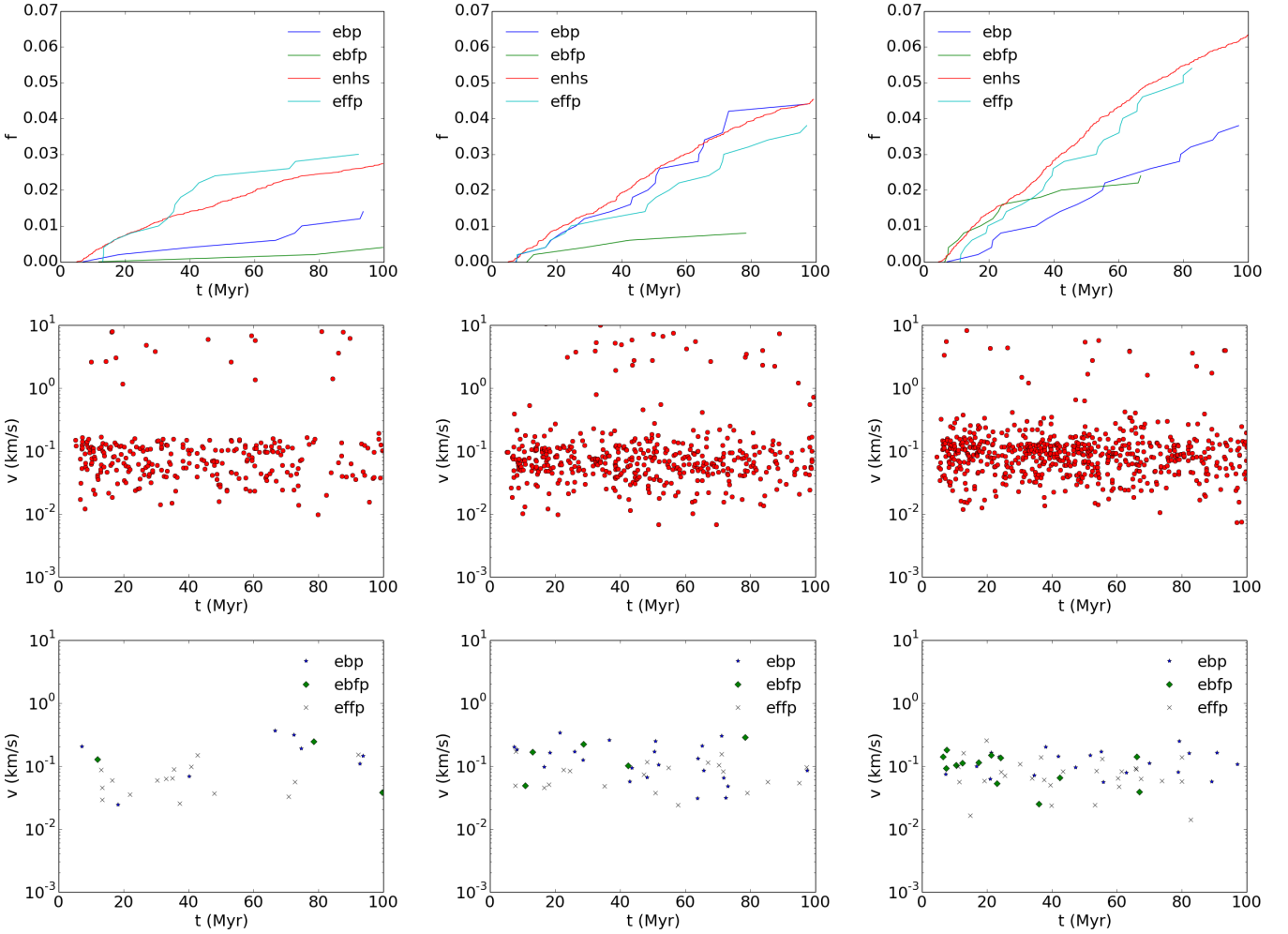
half-mass radius when  $t \lesssim t_{\text{rh}}$ . The star cluster relaxes and the  $r_{\text{hm}}$  evolves similarly in all the three models at subsequent times. The evolution of the core radius is more complex. In model C50M000, the core shrinks at  $t \approx t_{\text{rh}}$  and subsequently grows again at  $t \approx 2.5t_{\text{rh}}$ , as a result of mass segregation, followed by a core collapse (e.g., [Khalisi et al. 2007](#)). The core of model C50M000 enlarges after core collapse has occurred, and also ejects stars towards the outer regions of the cluster, reducing the total number of stars in the core. Although the core evolution appears steady during the first 100 Myr for the models containing an IMBH, the number of particles varies in the core until  $\sim 40$  Myr, leaving a small number of particle members for the remaining 60 Myr.

Figure 4 provides us insights on the evolution of the star cluster core. In model C50M00 (which does not contain an IMBH), the number of stars in the core, as well as the mass of the core, decreases substantially until the core collapses at  $t \approx 40$  Myr, and then rises again. In the models that contain a central IMBH, the number of stars in the core is substantially reduced, reaching a minimum of 0.1% of the total number of stars in model C50M100, and 0.03% for model C50M200. In general, the number of stars in the cluster core at any given time is smaller when a cluster has a more massive IMBH. The presence of an IMBH, however, appears to prevent the cluster core from collapsing, and a core with a more or less constant stellar density and mass density is maintained for long periods of time. In star cluster without an IMBH, dynamical interactions in the cluster core occur much faster in the timespan surrounding the core collapse. This state of high stellar density does not occur when a central IMBH is present, because of the quenched mass segregation. This phenomenon is described in [Gill et al. \(2008\)](#), who carried out a numerical investigation of the quenching mechanism in globular clusters, in which the IMBH prevents core collapse. Figure 5 shows the evolution of the ratio between the core radius and the half-mass radius for the three reference models. During the observational analysis of star clusters, the ratio between the core radius and the half-mass radius, combined with the ratios of the enclosed number of stars and the enclosed total mass in the cluster core, relative to those of the half-mass radius, can be used to identify when mass segregation has been quenched ([Gill et al. 2008](#)). Note that we have included stellar evolution, which may cause subtle differences between our results and those of [Gill et al. \(2008\)](#).

### 3.2.3 Escaping stars and planets

Here we analyse the escape rates of different populations in star clusters, with an emphasis on how they relate to the IMBH. Statistics on the escape fractions at  $t = 100$  Myr are listed in Table 3 for the different constituent populations of the star cluster. The gravitational potential evolves over time as a consequence of two-body relaxation, stellar evolution, and mass loss due to escaping stars. A central IMBH affects the gravitational potential of the star cluster directly (due to its presence in the centre of the star cluster), as well as indirectly (due to its effect on the dynamics of the stellar population, including quenching of mass segregation). This enhances both the ejection rates of stars and FFPs. The kinematics of the FFPs is primarily determined





**Figure 6.** Properties of the escaping particles for models C50M000 (*left*), C50M100 (*middle*), and C50M200 (*right*). The top row shows the cumulative distributions of the fraction of planetary systems, stars, and planets escaping from the star clusters (eBP/BP<sub>0</sub>, BFP/BP<sub>0</sub>, eBFP/BP<sub>0</sub>, and eFFP/FFP<sub>0</sub>; see Table 2). The middle and bottom rows show the velocity-at-infinity versus escape time for the escaping stars and for the escaping planets, respectively.

**Table 3.** The fraction of particles that have escaped at  $t = 100$  Myr, for different star clusters. The prefix "av" indicates the averaged results for the ensemble of simulations.

Model ID	eBP/BP <sub>0</sub>	BFP/BP <sub>0</sub>	eBFP/BP <sub>0</sub>	eNHS/N <sub>s0</sub>	eFFP/FFP <sub>0</sub>
C50M000	1.60 ± 0.56 %	8.80 ± 1.27 %	0.60 ± 0.34 %	2.78 ± 0.16 %	3.20 ± 0.79 %
C50M100	4.60 ± 0.94 %	10.80 ± 1.39 %	1.00 ± 0.45 %	4.58 ± 0.21 %	4.00 ± 0.88 %
C50M200	4.00 ± 0.88 %	10.20 ± 1.35 %	2.60 ± 0.71 %	6.42 ± 0.24 %	5.60 ± 1.03 %
avC50M000	1.82 ± 0.04 %	9.94 ± 0.04 %	1.30 ± 0.05 %	2.72 ± 0.02 %	2.24 ± 0.02 %
avC50M100	3.36 ± 0.04 %	11.68 ± 0.04 %	1.70 ± 0.04 %	4.01 ± 0.02 %	3.60 ± 0.03 %
avC50M200	3.64 ± 0.03 %	11.22 ± 0.04 %	2.22 ± 0.05 %	5.57 ± 0.02 %	5.52 ± 0.04 %

by the global properties of the star cluster's gravitational field (e.g., Wang et al. 2015a).

As compared to the model without an IMBH (model C50M000) at  $t = 100$  Myr, the ejected fraction of eFFPs is 60% higher in model C50M100 and 146% higher in model C50M200. The fractions of ejected stars is 48% and 107% higher in models C50M100 and C50M200, respectively. At the end of the simulations ( $t = 100$  Myr), the number of eBFPs is somewhat larger in star clusters containing an IMBH, by 17% and 13%, for models C50M100 and C50M200, respectively. In latter models, a larger fraction of

stars tends to migrate out of the star cluster centre, decreasing the stellar density and hence, also the close encounter rate. This effect is more prominent for clusters with higher-mass IMBHs. Most of the encounters involving a notable interaction with the IMBH occur before the central region expands. The fraction of BPs ejected in model C50M000 is comparable to that of the models of Flammini Dotti et al. (2019). The average number of ejected BPs at  $t = 100$  Myr is 83% and 100% higher, for models C50M100 and C50M200, respectively, as compared to model C50M000.

The distribution of escape times is shown in the top

panels of Figure 6. The escape rate of all populations is higher when a more massive IMBH is present. The escape rate of the different populations of particles is roughly constant with time. For model C50M000, half of the stars that are ejected during the simulation ( $t < 100$  Myr) are expelled from the cluster within  $\sim 50$  Myr. For models C50M100 and C50M200, these timescales are  $\sim 35$  Myr and  $\sim 20$  Myr for C50M200, respectively. The IMBH ejects most stars during the first few million years, resulting in a larger total number of ejections. High-mass stars tend to rapidly migrate to the cluster centre when no IMBH is present. When an IMBH is present, on the other hand, mass segregation is quenched, and many higher-mass stars are bounced out of the cluster core, the ejection rate may be somewhat higher.

Half of the eFFPs are produced within  $\sim 40$  Myr for model C50M000, while the corresponding timescales are 45 Myr and  $\sim 30$  Myr for models C50M100 and C50M200. The ejection of FFPs from the cluster is slowed down when an IMBH is present in the star cluster. The ejection rate of FFPs directly related to the evolution of the gravitational potential and the strength of the tidal field. However, the IMBH, both directly and indirectly, remains the major catalyst for the ejection of both stars and planets from the cluster. Unlike model C50M000, the production rate of eFFPs is roughly constant, for models C50M100 and C50M200.

The middle and bottom panels in Figure 6 show the escape speeds of stars and planets, respectively, as a function of the time at which each particle is identified as an escaper. The high-velocity single stars are ejected from the cluster core following strong scattering events with other stars and/of the IMBH (e.g., [Gvaramadze et al. 2009](#)), while low-velocity stellar and planetary escapers evaporate from the star cluster outskirts. As the cluster expands and gradually fills its Roche lobe, the tidal field gradually strips off stars from its outskirts. The number of stars that has escaped from the star cluster at  $t = t_{\text{th}}$  is higher in models containing a central IMBH. At this time, the fraction of stars that have escaped is  $\sim 1.3\%$ ,  $1.5\%$  and  $2.0\%$  of models C50M000, C50M100 and C50M200, respectively. Most stars and planets escape with speeds between  $0.01 \text{ km s}^{-1}$  and  $10 \text{ km s}^{-1}$ . As both stellar evolution and stellar escapers reduce the total mass of the star cluster, the gravitational potential is reduced and, consequently, the typical escape velocity also decreases slightly over time, while the stars passing through the core have their orbit augmented by the IMBH.

### 3.2.4 IMBH kinematics

The kinematics of an IMBH in a star cluster strongly affects the stellar and planetary populations. Shortly after we initialise the IMBH at rest at the cluster centre, the IMBH experiences recoils from gravitational interactions with other stars in the core of the star cluster. Figure 7 shows the kinematic properties of the IMBH in models C50M100 and C50M200 over time. The distance and speed of the IMBH are measured with respect the density centre of the star cluster.

The IMBHs in models C50M100 and C50M200 spend most of their time at respective distances of  $0.1 \text{ pc}$  and  $0.05 \text{ pc}$  from their cluster centres. Larger excursions are seen in model C50M100, where the IMBH is expelled two to a distance of  $\sim 0.4 \text{ pc}$  from the cluster centre. These larger dis-

**Table 4.** Fraction of the planetary systems in the star cluster that has remained intact (column 2), and the ratio of total number of free-floating planets, relative to the initial number of free-floating planets (column 3), at  $t = 100$  Myr.

Model ID	BP/BP <sub>0</sub> %	(FFP+BFP)/FFP <sub>0</sub> %
avC50M000	$88.24 \pm 0.04$	$105.95 \pm 0.03$
avC50M100	$84.96 \pm 0.04$	$106.38 \pm 0.03$
avC50M200	$85.14 \pm 0.03$	$103.48 \pm 0.03$

tances occur as a consequence of gravitational interactions with other massive objects in the star cluster. The IMBH in model C50M200 remains closer to the cluster core than that in model C50M100, due to the differences in inertia.

The typical speed of the IMBH during the simulation is  $0.059 \text{ km s}^{-1}$  in model C50M100 and  $0.075 \text{ km s}^{-1}$  in model C50M200. At early times ( $t \lesssim 10$  Myr) the star cluster is still compact and stellar encounters occur frequently, limiting the excursions in velocity of the IMBH. As these encounters become less frequent due to cluster expansion after 10 Myr, the IMBH is mostly subjected to the gravitational interaction with stars in the innermost regions of the star cluster, causing larger variations in its velocity. In model C50M200, there is a notable interaction with a binary companion, another  $68 M_{\odot}$  stellar-mass black hole at  $t \gtrsim 60$  Myr.

The tidal influence of an IMBH on planetary systems in the star cluster depends on the mass of the IMBH, but also strongly on their mutual distance. Whereas model C50M100 contains an IMBH that is only half the mass of that in C50M200, the motion of this IMBH ensures that also approaches many of the stars in the region beyond the core. The IMBH in model C50M100 experiences substantial scattering during the first few million years. Therefore, it only partially dominates the core structure, and is more subjected to stellar encounters. The latter can explain that the fraction of ejected planets in model C50M200 is slightly smaller than that in C50M100.

## 3.3 Kinematics of planetary systems and free-floating planets

### 3.3.1 Evolution of planetary systems

Small perturbations of outer planets in multi-planet systems can induce scattering events that result in the ejection of one or more planets from the system. As we only model single-planet systems in the present study, disruption of planetary systems through planet-planet scattering is not possible. Disruptions are thus always a direct consequence of (i) close encounters with neighbouring stars, and (ii) tidal interactions with the IMBH. The majority of the planetary systems remains intact during the entire simulation, but their orbits can be significantly perturbed. Figure 8 shows the correlations between the semi-major axis and eccentricity of planetary systems that have remained intact at  $t = 100$  Myr. As expected, the planets in long-period orbits typically experience the strongest perturbations. A comparison between the panels reveals that the direct effect of a central IMBH in the star cluster on the orbital elements of the BPs at  $t = 100$  Myr is not easily distinguishable in the population of surviving planetary systems. However, the IMBH does

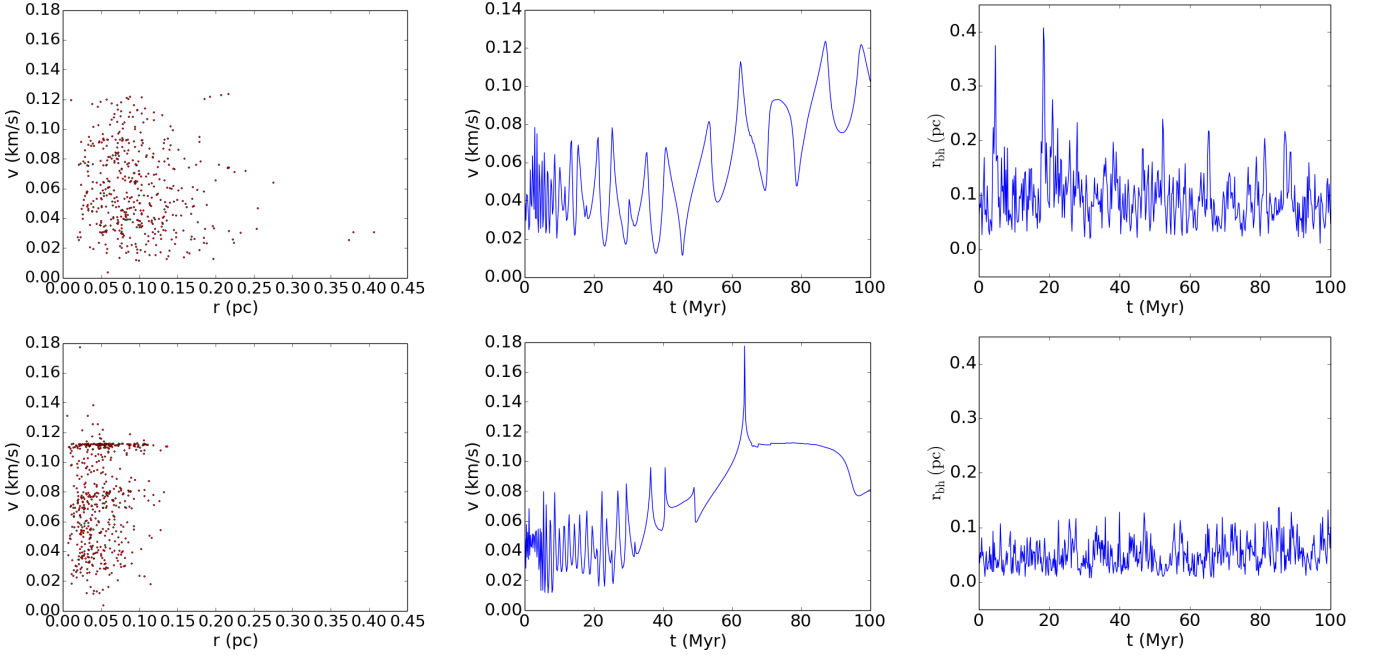


**Figure 7.** Kinematic properties of the IMBH over time, for models C50M100 (*top*) and C50M200 (*bottom*). *Left*: velocity versus distance from the star cluster centre; *middle*: velocity versus time; *right*: distance from the star cluster centre versus time.

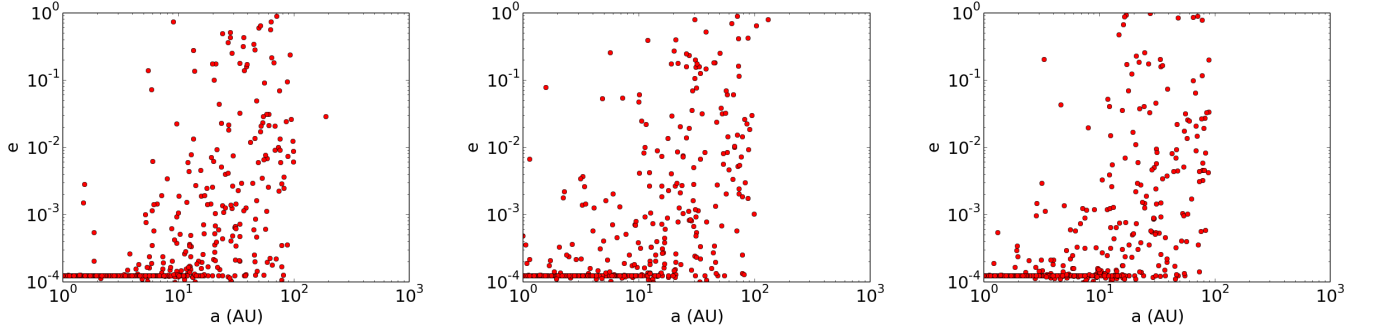


**Figure 8.** Correlations between semi-major axis and eccentricity, of all surviving planetary systems in the star cluster at  $t = 100$  Myr, for models C50M000 (*left*), C50M100, (*middle*) and C50M200 (*right*).

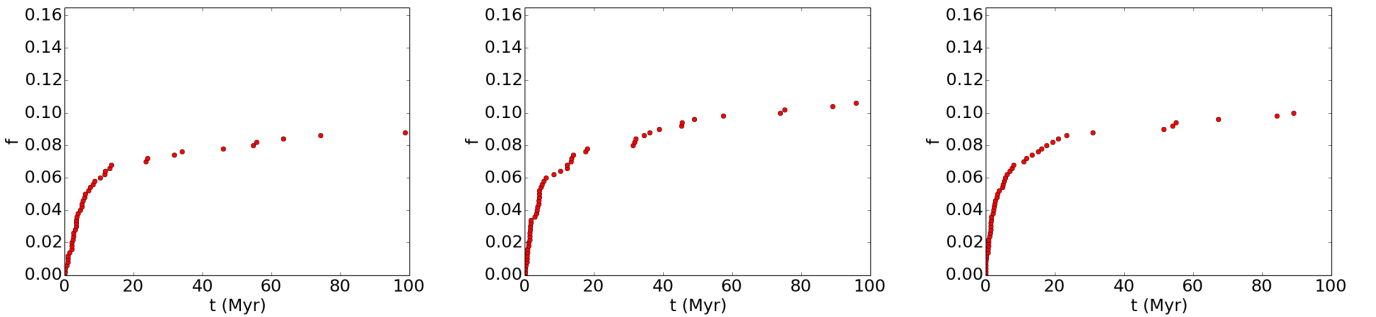


**Figure 9.** The cumulative fraction BFP/BP<sub>0</sub> during the simulation for models C50M000 (*left*), C50M100, (*middle*) and C50M200 (*right*).

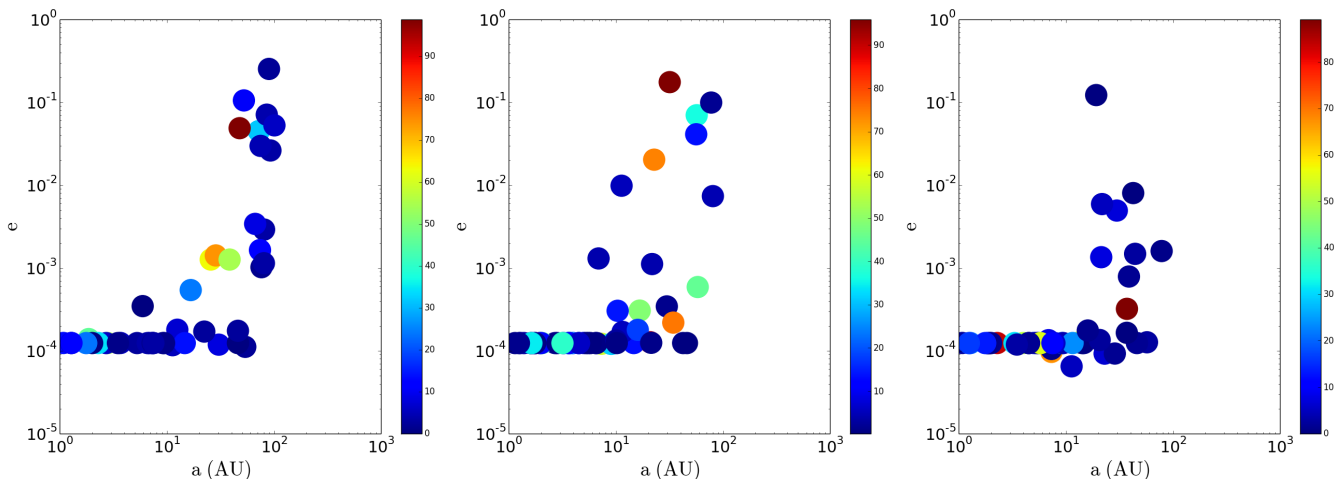


**Figure 10.** Semi-major axes and eccentricities of all disrupted planetary systems (the BPs), immediately before the the disruption event. The colour of each dot represents the disruption time in units of Myr. *Left:* model C50M000; *middle:* model C50M100; *right:* model C50M200.

leave an imprint in the survival fraction, and the population of disrupted planetary system, as discussed below.

Figure 9 shows the cumulative fraction of the times at which BFPs appear in the simulations (i.e., when planetary systems are disrupted). Most disruptions occur within one relaxation time, when the star cluster is compact and when the IMBH strongly influences the dynamics of both the stellar and the planetary populations. We estimate that a  $1M_{\odot}$  star in model C50M000 undergoes an encounter within a distance of 1000 AU every  $t_{\text{enc}} \approx 5.3$  Myr. The corresponding encounter frequencies are 5.1 Myr and 4.9 Myr for models C50M100 and C50M200, respectively (see also Malmberg et al. 2007). Of the total number of planetary systems disrupted during the entire simulation (i.e., 100 Myr), half are disrupted within the first  $\sim 6$  Myr,  $\sim 6$  Myr, and  $\sim 4$  Myr for models C50M000, C50M100 and C50M200, respectively.

Table 4 shows that in the models that contain an IMBH, the number of planetary systems in the star cluster is reduced by approximately 16%, due to escape of planetary systems from the star cluster ( $\approx 4\%$ ), and due to disruptions of planetary systems ( $\approx 12\%$ ). In model without a central IMBH, on the other hand, the number of planetary systems is reduced by approximately only 11%. In models containing an IMBH, mass segregation quenching prevents the star cluster core from losing the majority of its members during the early phases of the star cluster dynamical evolution (see Figure 4). After the first 10 Myr, the star cluster expands and starts to slowly fill its Roche Lobe. At  $t \approx t_{\text{rh}}$ , the disruption rate of planetary systems drops significantly, and the three models have a similar, more or less constant ejection rate.

Figure 10 shows the orbital elements of the planetary systems at the time-step prior to disruption of the system, with colours indicating the time of ejection. There is a non-negligible percentage of 1 – 10 AU planets ejected from their host stars, while the 10 – 100 AU region is of more difficult interpretation, as the star cluster density can strip those planets easier. The majority of these, which semi-major axis is below 10 AU, escape before 10 Myr, while most of the BFP escape before 30 Myr. The presence of a central IMBH

in the star cluster enhances the fraction of BFPs originating from systems with  $a = 1 - 10$  AU by 13 – 16%, as compared to the model without an IMBH. Therefore, a central IMBH enhances the disruption of short-period planets. The total number of BFP, coming from the semi-major axis interval 1 – 10 AU, is enhanced by  $\sim 2\%$  from model C50M000 to C50M100. These results suggest that planetary systems with small semi-major axes are disrupted more easily in star clusters containing an IMBH as compared to in star clusters without an IMBH.

The third column of Table 4 shows the ratio of the total number of free-floating planets (BFP+FFP) in the cluster, as compared to its initial value (FFP<sub>0</sub>), at  $t = 100$  Myr. The number of BFPs is higher for models containing an IMBH, due to the disruption of planetary systems. The ejection rate of FFPs, on the other hand, is also higher when a central IMBH is present. Hence, the highest number of free-floating planets (BFP+FFP) can be found in model C50M100.

### 3.3.2 Density profiles and IMBH effects on planetary systems

The stellar density is among the most important parameters that determines the stability of planetary systems. To investigate the effect of stellar density, we carry out simulations of star clusters with different initial stellar densities. We carry out simulations with  $N_s = 5000$ , 10000 and 15000 stars, while retaining the same initial half-mass radius as in our reference model. We label these models with the template C-Q0-IMBH-mass, with a postfix "d0", "d1" or "d2", corresponding to the models with  $N_s = 5000$ , 10000 and 15000 respectively.

As can be seen in Table 5 and Figure 11, the number of BFPs increases with increasing stellar cluster density. Mass segregation is quenched in all models containing an IMBH. However, a larger stellar density results in a higher rate of close encounters between stars. The total mass star clusters C50M000d0, C50M100d0, and C50M200d0 is approximately half of the mass of the corresponding reference models. Due to their shallower gravitational potential well, these clusters



**Table 5.** The fraction of the planets in the star that have escaped from their host stars that is located in the star cluster (BFP) or outside the star cluster (eBFP), and fraction of the initially free-floating planets that has escaped from the star cluster, for star clusters with different initial masses, at  $t = 100$  Myr. The density model (dn) is indicated at the top of each column, with "d0", "d1", and "d2" for  $N_s = 5000$ , 10 000, and 15 000, respectively.

ID	Quantity	d0 ( $N_s = 5000$ )	d1 ( $N_s = 10000$ )	d2 ( $N_s = 15000$ )
C50M000dn	BFP/BP <sub>0</sub>	$4.8 \pm 0.9$ %	$9.9 \pm 1.3$ %	$12.8 \pm 1.5$ %
	eBFP/BP <sub>0</sub>	$1.0 \pm 0.4$ %	$1.3 \pm 0.5$ %	$1.4 \pm 0.5$ %
	eFFP/FFP <sub>0</sub>	$3.2 \pm 0.8$ %	$2.2 \pm 0.6$ %	$2.2 \pm 0.7$ %
	$r_c$	0.34 pc	0.39 pc	0.29 pc
	$r_{hm}$	0.80 pc	0.78 pc	0.80 pc
C50M100dn	BFP/BP <sub>0</sub>	$6.0 \pm 1.1$ %	$11.5 \pm 1.4$ %	$16.0 \pm 1.6$ %
	eBFP/BP <sub>0</sub>	$2.0 \pm 0.6$ %	$1.7 \pm 0.6$ %	$2.2 \pm 0.7$ %
	eFFP/FFP <sub>0</sub>	$5.0 \pm 1.0$ %	$3.6 \pm 0.8$ %	$2.2 \pm 0.7$ %
	$r_c$	0.19 pc	0.24 pc	0.15 pc
	$r_{hm}$	0.83 pc	0.79 pc	0.81 pc
C50M200dn	BFP/BP <sub>0</sub>	$8.2 \pm 1.2$ %	$11.2 \pm 1.4$ %	$16.2 \pm 1.6$ %
	eBFP/BP <sub>0</sub>	$1.4 \pm 0.5$ %	$2.2 \pm 0.6$ %	$2.6 \pm 0.7$ %
	eFFP/FFP <sub>0</sub>	$5.6 \pm 1.0$ %	$5.5 \pm 1.0$ %	$3.0 \pm 0.8$ %
	$r_c$	0.11 pc	0.15 pc	0.09 pc
	$r_{hm}$	0.86 pc	0.80 pc	0.82 pc

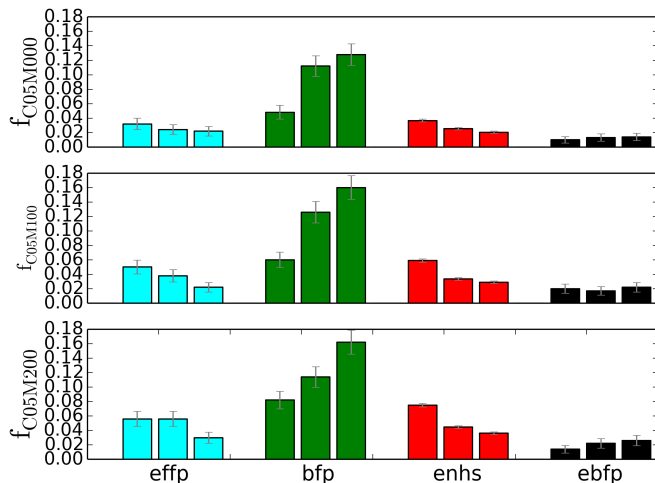


**Figure 11.** Fractions eFFP/FFP<sub>0</sub>, BFP/BP<sub>0</sub>, eNHS/NHS<sub>0</sub> and eBFP/BP<sub>0</sub> escaped from the star cluster fraction, at  $t = 100$  Myr, for models C50M000 (*top*), C50M100 (*middle*) and C50M200 (*right*).

have, on average, a higher production rate of eFFPs. The number of ejected stars is numerically larger in denser star clusters (since  $N_s$  is larger), although the fraction of stars that is ejected from the star clusters is lower. For the same reason, models C50M000d2, C50M100d2, and C50M200d2, are similarly influenced by the IMBH in its core and the intermediate regions within the  $r_{hm}$ , which becomes more populated.

Figure 12 provides us important insights into the disruption mechanisms of planetary system in a more and less dense star cluster. When comparing Figures 9 and 12, we can see that the fraction of BFP depends strongly on both the presence of an IMBH, as well as the star cluster density. Half of the planetary systems are disrupted before 7 Myr for model C50M100d0 and 6 Myr for model C50M200d0. The same fraction of planetary systems is disrupted in less than 1 Myr in the denser models C50M100d2 and C50M200d2.

The star cluster density and IMBH tidal effect are intrinsically connected. The IMBH's tidal field enhances the stellar velocities in its neighbourhood, and in a denser star cluster, encounters occur more frequently, and there are more ejections than in star clusters with a lower stellar density.

### 3.3.3 Dependence on initial semi-major axis distribution

We study how the star-planet systems with different semi-major axes evolve, in order to understand the implications of the IMBH contribution for the evolution and disruption rates of short-period planetary systems. We study star-planet systems with semi-major axes distributions drawn from uniform log-normal distributions in the range 1–10 AU (models "a0"), 1–100 AU (models "a1" as in the reference models) and 10–100 AU (models "a2"); see Table 6. In star clusters similar to those in our simulations, the critical value of  $a = 10$  AU separates two different probability ejection regimes (e.g., Fujii & Hori 2019; Flammini Dotti et al. 2019).

The blue dots in Figure 13 represent the 1–10 AU semi-major axis interval, and are consistent with the results of Flammini Dotti et al. (2019) and Fujii & Hori (2019). The fraction of disrupted planetary systems is again larger than in the model without an IMBH, by 100% and 133% in models C50M100a0 and C50M200a0, respectively. The red dots in Figure 13 represent 10–100 AU semi-major axis interval, and exhibit a similar behaviour as in Figure 12. Planets with larger semi-major axes have a larger probability of being ejected both due to stellar encounters, combined with the tidal influence of the IMBH. It is difficult to disentangle the relative contributions of these two processes. In Table 6 and Figure 14, we obtain similar results as Fujii & Hori (2019); Flammini Dotti et al. (2019). When comparing the different models, the number of disrupted planetary systems (BFPs) is large for the 10–100 AU interval, while it remains small for the 1–10 AU. Planetary systems with  $a \lesssim 10$  AU (Saturn's orbit) are relatively difficult to disrupt, unless these are multi-planet systems, in which planet-planet scattering can occur. The necessary conditions related to velocity of both host star and encountering star are more likely

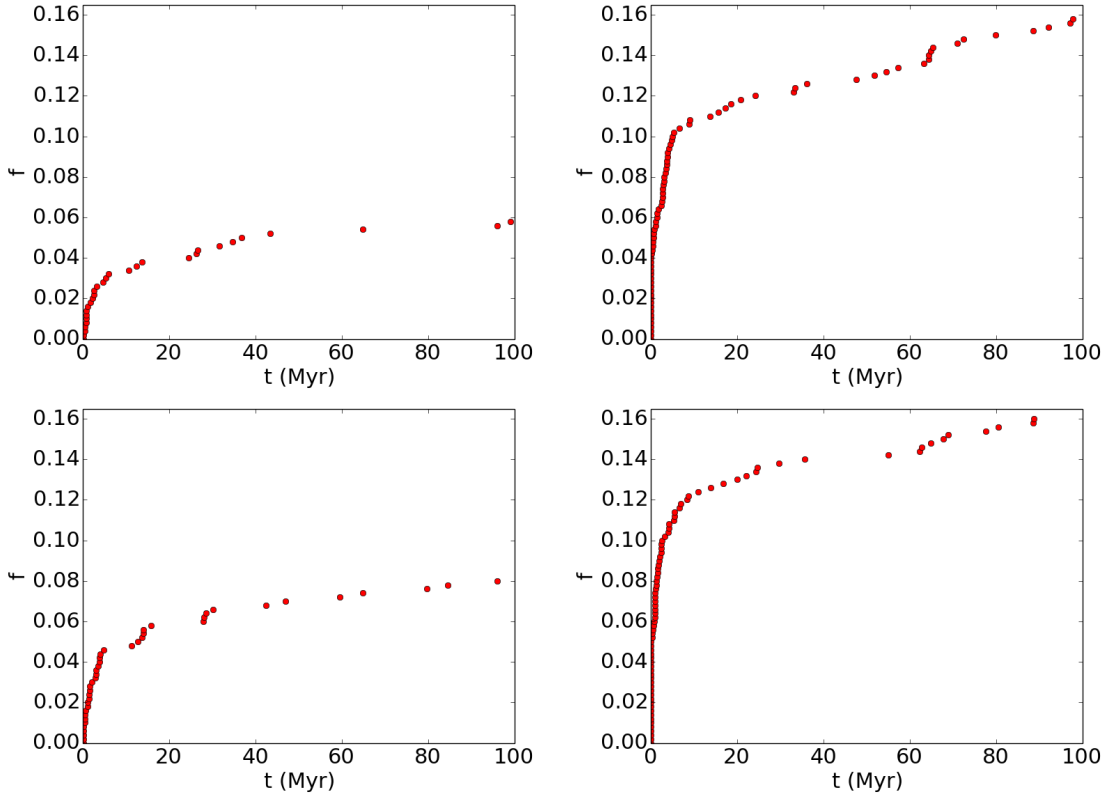


**Figure 12.** The cumulative fraction BFP/BP<sub>0</sub> generated in the star cluster, for models C50M100d0 (*top-left*), C50M200d0 (*bottom-left*), C50M100d2 (*top-right*) and C50M200d2 (*bottom-right*).

**Table 6.** Fractions of BFPs and eBFPs for models with different initial semi-major axis intervals, at  $t = 100$  Myr. The models are indicated in the first column, with  $an$  indicating the initial semi-major axis interval ("a0", "a1", and "a2" for 1 – 10 AU, 1 – 100 AU and 10 – 100 AU, respectively) in columns 2 – 7. Columns 8 and 9 lists the core radii and half-mass radii, respectively.

Model ID	a0 (1 – 10 AU)		a1 (1 – 100 AU)		a2 (10 – 100 AU)		$r_c$ pc	$r_{hm}$ pc
	BFP/BP <sub>0</sub>	eBFP/BP <sub>0</sub>	BFP/BP <sub>0</sub>	eBFP/BP <sub>0</sub>	BFP/BP <sub>0</sub>	eBFP/BP <sub>0</sub>		
C50M000 $an$	$0.6 \pm 0.3$ %	$0.2 \pm 0.2$ %	$9.9 \pm 1.3$ %	$1.3 \pm 0.5$ %	$21.4 \pm 1.8$ %	$2.0 \pm 0.6$ %	0.39	0.78
C50M100 $an$	$1.2 \pm 0.5$ %	$0.4 \pm 0.3$ %	$11.6 \pm 1.4$ %	$1.7 \pm 0.6$ %	$21.0 \pm 1.8$ %	$2.8 \pm 0.7$ %	0.24	0.79
C50M200 $an$	$1.4 \pm 0.5$ %	$0.4 \pm 0.3$ %	$11.2 \pm 1.4$ %	$2.2 \pm 0.6$ %	$23.2 \pm 1.9$ %	$4.2 \pm 0.9$ %	0.15	0.80

to be reached inside the core, rather than outside. On the 10 – 100 AU interval we have a different situation. Planets are far more easy to be ejected, also through average close encounter.

#### 4 DISCUSSION AND CONCLUSIONS

We have numerically investigated the influence of a central IMBH on the dynamical evolution of planetary systems and free-floating planets in star clusters. We provide analytic estimates for the tidal force exerted on planetary systems by the IMBH, as compared to that of the nearest neighbour stars. We characterise survival rates of planetary systems, and escape rates of stars, planetary systems, and free-floating planets, as a function of time, IMBH mass, the initial stellar density, and the initial planetary semi-major axis distribution. Our findings can be summarised as follows.

(i) Planetary systems experience a tidal force of neighbouring stars and of the central IMBH. Depending on the

density profile of the star cluster, the IMBH's tidal force dominates over that of nearest neighbour stars in large regions of the star cluster. In the Plummer model, a central IMBH with a mass larger than 3.4% of the total stellar mass dominates the tidal force throughout the entire star cluster. A central IMBH exerts a continuous tidal force on all planetary systems in the star cluster, while close encounters with nearby neighbours can have substantial short-term effects. Finally, it is rather unlikely that the IMBH will directly strip the host star of its planet. The IMBH is in the core, therefore there is a larger probability of an encounter that destroys the planetary system before it reaches the IMBH.

(ii) Gravitational interactions with neighbouring stars affect planetary systems in star clusters, and the IMBH enhances these effects. Moreover, we find that the IMBH has the most prominent effect during the early and more compact phases of the star cluster life. The escape rate of both stars and planets in the star cluster is higher when an IMBH is present in the star cluster.

(iii) The quenched mass segregation mechanism modifies

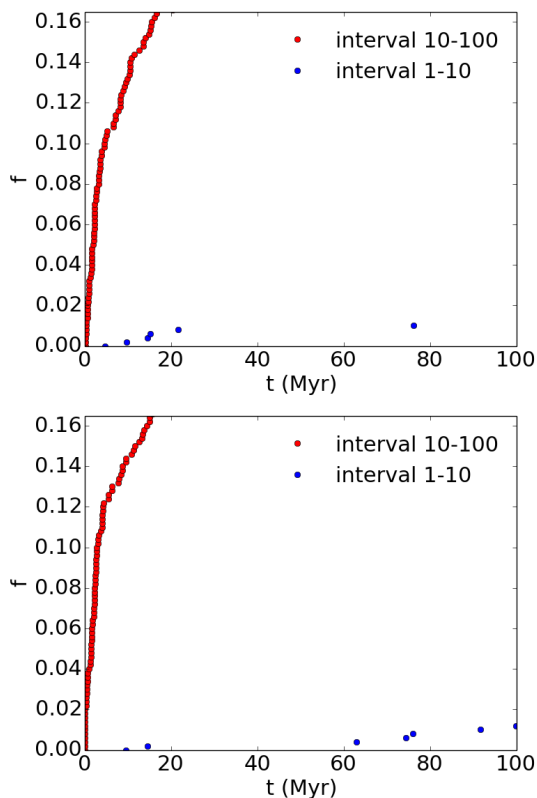


**Figure 13.** The cumulative fraction BFP/BP<sub>0</sub> for models C50M100a0 and C50M100a2 (*top*) and for models C50M200a0 and C50M200a2 (*bottom*).

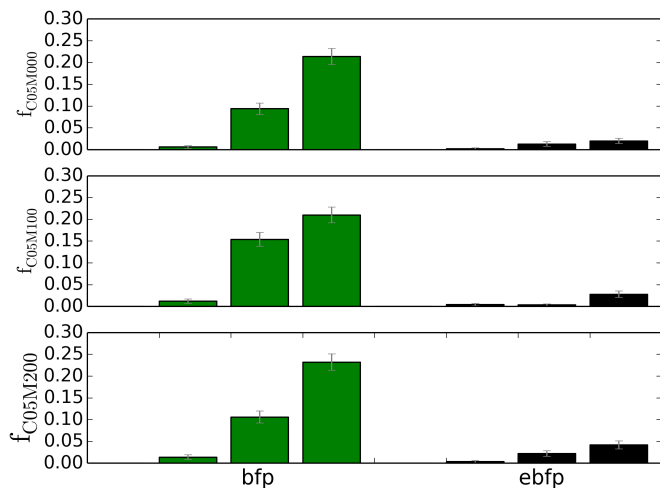


**Figure 14.** Fractions BFP/BP<sub>0</sub> (green bars) and eBFP/BP<sub>0</sub> (black bars) at  $t = 100$  Myr, for different initial semi-major axis distributions. From left to right, the bars in each group represent initial semi-major axis distributions in the range 1 – 10 AU, 1 – 100 AU, and 10 – 100 AU, respectively, for models C50M000 (*top*), C50M100 (*middle*) and C50M200 (*bottom*).

the evolution of the star cluster, in the presence of a central IMBH. The stars are bounced back from the star cluster core, resulting in a relatively poor core population, from which the more massive stars are also regularly ejected, and more stars in the intermediate region within the  $r_{\text{hm}}$ .

(iv) The kinematics of free-floating planets (BFPs and FFPs) is mostly affected by the gradual change in the star cluster’s global gravitational potential. The effect of a central IMBH on stellar ejection rates and reshaping of the cluster’s density profile, combined with stellar evolution, determines the ejection rates of the free-floating planets.

(v) The amplitude of the motion of the IMBH in the star cluster core due to interactions with stars in the cluster core is smaller for higher-mass IMBHs. As the location of the IMBH in the star cluster determines the dynamics of the neighbouring population, and also the tidal effect on planetary systems, this behaviour may justify the slightly larger number of disrupted planetary systems in the models with a  $100M_{\odot}$  IMBH, as compared to the  $200M_{\odot}$  IMBH.

(vi) The rate of planetary system disruptions (and consequently, the fraction of BFP in the cluster) is higher when an IMBH is present. The IMBH enhances the velocities of the stars passing near it and enhance the close encounter ratio in the star cluster. The production rates of BFPs and eFFPs are numerically larger in models containing a central IMBH, as compared to star clusters without an IMBH. The trend is confirmed for different star cluster densities and, for BFP, for models with different initial semi-major axis intervals as well.

(vii) All particles in the star cluster are directly or indirectly affected by the IMBH. This affect is most important during the first  $\sim 10$  Myr, until the star cluster fills its Roche lobe. The planets ejected from their host star are affected on all the tested semi-major axis. Even for planets in short-period orbits ( $a < 10$  AU), there is a, non-negligible, additional contribution of ejected planets when an IMBH is present in the cluster.

(viii) Within a timescale of 100 Myr, star cluster with a higher initial stellar density have a higher disruption rate of planetary systems, due to the increased frequency of close encounters, and a reduced production rate of ejected free-floating planets, due to the deeper gravitational potential.

Our study highlights the importance of an IMBH when considering planetary systems in star clusters. Although the presence of IMBHs in the centres of star clusters has not yet been unambiguously determined, continued observational efforts are likely to reveal their presence in the coming decade. Aside from observational work, further computational efforts are also necessary to characterise the influence of IMBHs with a wide range of masses on multi-planet systems in globular clusters.

## ACKNOWLEDGEMENTS

We are grateful to the anonymous referee for providing comments and suggestions that helped to improve this paper. F.F.D. acknowledges support from the XJTLU postgraduate research scholarship. M.B.N.K. acknowledges support from the National Natural Science Foundation of China (grant 11573004). This research was supported by the Research

Development Fund (grant RDF-16-01-16) of Xi'an Jiaotong-Liverpool University (XJTLU). We acknowledge the support of the DFG priority program SPP 1992 "Exploring the Diversity of Extrasolar Planets (Sp 345/20-1)". We thank Zhongmu Li of Dali University, Yunnan, China for the organization, kind hospitality and support during a workshop in Dali in 2019 and Hyung Mok Lee and the Korea Astronomy and Space Science Institute (KASI) in Daejeon, Korea (Rep.), for financial support during the KCK11 meeting in Dec. 2019. This work has been partly supported by Sino-German cooperation (DFG, NSFC) under project number GZ 1284. We are grateful to Martin Gorbahn for discussions that helped to improve the paper.

## DATA AVAILABILITY

The data underlying this article will be shared on reasonable request to the corresponding author.

## REFERENCES

- Aarseth S. J., 1999, *Celest. Mech. Dyn. Astron.*, **73**, 127
- Aarseth S. J., 2001, *New Astron.*, **6**, 277
- Aarseth S. J., 2010, *Gravitational N-Body Simulations*. Cambridge Monographs on Mathematical Physics
- Abbott B. P., et al., 2017, *ApJ*, **848**, L12
- Abe F., et al., 2004, *Science*, **305**, 1264
- Ahmad A., Cohen L., 1973, *Journal of Computational Physics*, **12**, 389
- Arca-Sedda M., 2016, *MNRAS*, **455**, 35
- Banerjee S., 2020, arXiv e-prints, p. arXiv:2004.07382
- Beaulieu J.-P., et al., 2006, *Nature*, **439**, 437
- Belczynski K., Kalogera V., Bulik T., 2002, *ApJ*, **572**, 407
- Belczynski K., Kalogera V., Rasio F. A., Taam R. E., Zezas A., Bulik T., Maccarone T. J., Ivanova N., 2008, *ApJS*, **174**, 223
- Binney J., Tremaine S., 2008, *Galactic Dynamics: Second Edition*. Princeton University Press
- Boley A. C., Payne M. J., Ford E. B., 2012, *ApJ*, **754**, 57
- Cai M. X., Meiron Y., Kouwenhoven M., Assmann P., Spurzem R., 2015, *ApJ*, **219**, 12
- Cantrell A. G., et al., 2010, *ApJ*, **710**, 1127
- Casertano S., Hut P., 1985, *ApJ*, **298**, 80
- Craig J., Krumholz M. R., 2013, *ApJ*, **769**, 150
- Delorme P., et al., 2012, *A&A*, **548**, A26
- Farrell S. A., Webb N. A., Barret D., Godet O., Rodrigues J. M., 2009, *Nature*, **460**, 73
- Flammini Dotti F. F., Kouwenhoven M. B. N., Cai M. X., Spurzem R., 2019, *MNRAS*, **489**, 2280
- Flammini Dotti F., Cai M. X., Spurzem R., Kouwenhoven M. B. N., 2020, in Elmegreen B. G., Tóth L. V., Güdel M., eds, *IAU Symposium Vol. 345, IAU Symposium*. pp 293–294
- Freitag M., Amaro-Seoane P., Kalogera V., 2006, *ApJ*, **649**, 91
- Fryer C. L., 1999, *ApJ*, **522**, 413
- Fujii M. S., Hori Y., 2019, *A&A*, **624**, A110
- Gaudi B. S., 2012, *ARA&A*, **50**, 411
- Giersz M., Spurzem R., 1994, *MNRAS*, **269**, 241
- Gill M., Trenti M., Miller M. C., van der Marel R., Hamilton D., Stiavelli M., 2008, *ApJ*, **686**, 303
- Gould A., Loeb A., 1992, *ApJ*, **396**, 104
- Gürkan M. A., Freitag M., Rasio F. A., 2004, *ApJ*, **604**, 632
- Gvaramadze V. V., Gualandris A., Portegies Zwart S., 2009, *MNRAS*, **396**, 570
- Haiman Z., Thoul A. A., Loeb A., 1996, *ApJ*, **464**, 523
- Hao W., Kouwenhoven M. B. N., Spurzem R., 2013, *MNRAS*, **433**, 867
- Heggie D., Hut P., 2003, *Classical and Quantum Gravity*, **20**, 4504
- Hobbs G., Lorimer D. R., Lyne A. G., Kramer M., 2005, *MNRAS*, **360**, 974
- Hurley J. R., 2007, *MNRAS*, **379**, 93
- Hurley J. R., Shara M. M., 2002, *ApJ*, **565**, 1251
- Hurley J. R., Pols O. R., Tout C. A., 2000, *MNRAS*, **315**, 543
- Hurley J. R., Tout C. A., Pols O. R., 2002, *MNRAS*, **329**, 897
- Hurley J. R., Pols O. R., Aarseth S. J., Tout C. A., 2005, *MNRAS*, **363**, 293
- Hurley J. R., Aarseth S. J., Shara M. M., 2007, *ApJ*, **665**, 707
- Hurley J. R., Tout C. A., Pols O. R., 2013b, BSE: Binary Star Evolution, Astrophysics Source Code Library (ascl:1303.014)
- Hurley J. R., Pols O. R., Tout C. A., 2013a, SSE: Single Star Evolution, Astrophysics Source Code Library (ascl:1303.015)
- Khalisi E., Amaro-Seoane P., Spurzem R., 2007, *MNRAS*, **374**, 703
- Koliopanos F., 2017, in *Proceedings of the XII Multifrequency Behaviour of High Energy Cosmic Sources Workshop*. 12–17 June, 2017 Palermo, Italy (MULTIF2017). p. 51 (arXiv:1801.01095)
- Kouwenhoven M. B. N., Goodwin S. P., Parker R. J., Davies M. B., Malmberg D., Kroupa P., 2010, *MNRAS*, **404**, 1835
- Kroupa P., 2001, *MNRAS*, **322**, 231
- Kulkarni S. R., Hut P., McMillan S., 1993, *Nature*, **364**, 421
- Lada C. J., Lada E. A., 2003, *ARA&A*, **41**, 57
- Lamers H. J. G. L. M., Gieles M., Portegies Zwart S. F., 2005, *A&A*, **429**, 173
- Lin D., et al., 2020, *ApJ*, **892**, L25
- Liu M. C., et al., 2013, *ApJ*, **777**, L20
- Ma S., Mao S., Ida S., Zhu W., Lin D. N. C., 2016, *MNRAS*, **461**, L107
- Madau P., Rees M. J., 2001, *ApJ*, **551**, L27
- Malmberg D., de Angeli F., Davies M. B., Church R. P., Mackey D., Wilkinson M. I., 2007, *MNRAS*, **378**, 1207
- Malmberg D., Davies M. B., Heggie D. C., 2011, *MNRAS*, **411**, 859
- Mao S., Paczynski B., 1991, *ApJ*, **374**, L37
- Mardling R. A., Aarseth S. J., 2001, *MNRAS*, **321**, 398
- Mayo A. W., Vanderburg A., et al 2018, *ApJ*, **136**, 25
- Miller M. C., Hamilton D. P., 2002, *MNRAS*, **330**, 232
- Moeckel N., Clarke C. J., 2011, *MNRAS*, **415**, 1179
- Mouri H., Taniguchi Y., 2002, *ApJ*, **580**, 844
- Mróz P., et al., 2017, *Nature*, **548**, 183
- Muzić K., Scholz A., Geers V. C., Jayawardhana R., 2015, *ApJ*, **810**, 159
- Ninkovic S., 1985, *Astronomische Nachrichten*, **306**, 237
- Parker R. J., Quanz S. P., 2012, *MNRAS*, **419**, 2448
- Peña Ramírez K., Béjar V. J. S., Zapatero Osorio M. R., Petr-Gotzens M. G., Martín E. L., 2012, *ApJ*, **754**, 30
- Perera B. B. P., et al., 2017, *MNRAS*, **468**, 2114
- Perets H. B., Kouwenhoven M. B. N., 2012, *ApJ*, **750**, 83
- Plummer H. C., 1911, *MNRAS*, **71**, 460
- Portegies Zwart S. F., McMillan S. L. W., 2002, *ApJ*, **576**, 899
- Portegies Zwart S. F., Baumgardt H., Hut P., Makino J., McMillan S. L. W., 2004, *Nature*, **428**, 724
- Portegies Zwart S. F., McMillan S. L. W., Gieles M., 2010, *ARA&A*, **48**, 431
- Portell de Mora J., García-Berro E., Estepa C., Castañeda J., Clotet M., 2011, in *High-Performance Computing in Remote Sensing*. p. 818305, doi:10.1117/12.898203
- Reinoso B., Schleicher D. R. G., Fellhauer M., Klessen R. S., Boekholt T. C. N., 2018, *A&A*, **614**, A14
- Ricotti M., Ostriker J. P., 2004, *MNRAS*, **352**, 547
- Schödel R., et al., 2002, *Nature*, **419**, 694
- Scholz A., Jayawardhana R., Muzic K., Geers V., Tamura M., Tanaka I., 2012, *ApJ*, **756**, 24



- Sigurdsson S., Hernquist L., 1993, *Nature*, **364**, 423
- Spitzer L., 1987, *Dynamical evolution of globular clusters*. Princeton University press
- Spurzem R., 1999, *Journal of Computational and Applied Mathematics*, **109**, 407
- Spurzem R., Takahashi K., 1995, *MNRAS*, **272**, 772
- Spurzem R., Giersz M., Heggie D. C., Lin D. N. C., 2009, *ApJ*, **697**, 458
- Strigari L. E., Barnabè M., Marshall P. J., Blandford R. D., 2012, *MNRAS*, **423**, 1856
- Sumi T., et al., 2011, *Nature*, **473**, 349
- Tapamo H., 2009, in Gracia J., de Colle F., Downes T., eds, *Lecture Notes in Physics*, Berlin Springer Verlag Vol. 791, *Jets From Young Stars V.* p. 3, doi:10.1007/978-3-642-03370-4\_1
- Thompson S., et al., 2018, *ApJ*, **235**, 49
- Veras D., Raymond S. N., 2012, *MNRAS*, **421**, L117
- Wang L., Kouwenhoven M. B. N., Zheng X., Church R. P., Davies M. B., 2015a, *MNRAS*, **449**, 3543
- Wang L., Spurzem R., Aarseth S., Nitadori K., Berczik P., Kouwenhoven M. B. N., Naab T., 2015b, *MNRAS*, **450**, 4070
- Wang L., et al., 2016, *MNRAS*, **458**, 1450
- Wheeler J. C., Johnson V., 2011, *ApJ*, **738**, 163
- Wilkinson M. I., Hurley J. R., Mackey A. D., Gilmore G. F., Tout C. A., 2003, *MNRAS*, **343**, 1025
- Wrobel J. M., Miller-Jones J. C. A., Middleton M. J., 2016, *AJ*, **152**, 22
- Yoshida N., Abel T., Hernquist L., Sugiyama N., 2003, *ApJ*, **592**, 645
- de Vita R., Trenti M., MacLeod M., 2018, *MNRAS*, **475**, 1574
- den Brok M., et al., 2015, *ApJ*, **809**, 101